# Classes of Hydrodynamic and Magnetohydrodynamic Turbulent Decay

Axel Brandenburg[1,2,3,4,*] and Tina Kahniashvili[5,6,7,†]

[1]Laboratory for Atmospheric and Space Physics, University of Colorado, Boulder, Colorado 80303, USA
[2]JILA and Department of Astrophysical and Planetary Sciences, University of Colorado, Boulder, Colorado 80303, USA
[3]Nordita, KTH Royal Institute of Technology and Stockholm University, Roslagstullsbacken 23, 10691 Stockholm, Sweden
[4]Department of Astronomy, AlbaNova University Center, Stockholm University, 10691 Stockholm, Sweden
[5]The McWilliams Center for Cosmology and Department of Physics, Carnegie Mellon University, 5000 Forbes Avenue, Pittsburgh, Pennsylvania 15213, USA
[6]Department of Physics, Laurentian University, Ramsey Lake Road, Sudbury, ON P3E 2C, Canada
[7]Abastumani Astrophysical Observatory, Ilia State University, 3-5 Cholokashvili Ave, Tbilisi, GE-0194, Georgia

(Received 5 July 2016; published 3 February 2017)

We perform numerical simulations of decaying hydrodynamic and magnetohydrodynamic turbulence. We classify our time-dependent solutions by their evolutionary tracks in parametric plots between instantaneous scaling exponents. We find distinct classes of solutions evolving along specific trajectories toward points on a line of self-similar solutions. These trajectories are determined by the underlying physics governing individual cases, while the infrared slope of the initial conditions plays only a limited role. In the helical case, even for a scale-invariant initial spectrum (inversely proportional to wave number $k$), the solution evolves along the same trajectory as for a Batchelor spectrum (proportional to $k^4$).

DOI: 10.1103/PhysRevLett.118.055102

The study of decaying turbulence is as old as that of turbulence itself. Being independent of an ill-defined forcing mechanism, decaying turbulence has a better chance in displaying generic properties of turbulence. Such properties are usually reflected in the existence of conserved quantities such as the Loitsiansky integral [1] and the magnetic helicity [2,3]. Important applications of decaying turbulence include grid turbulence [4], turbulent wakes [5], atmospheric turbulence [6], as well as interstellar turbulence [7], galaxy clusters [8], and the early Universe [9,10]. In the latter case, cosmological magnetic fields generated in the early Universe provide the initial source of turbulence, which leads to a growth of the correlation length by an inverse cascade mechanism [11], in addition to the general cosmological expansion of the Universe. In the last two decades, this topic has gained significant attention [12]. The time span since the initial magnetic field generation is enormous, but it is still uncertain whether it is long enough to produce fields at sufficiently large length scales to explain the possibility of contemporary magnetic fields in the space between clusters of galaxies [13].

In this Letter, we use direct numerical simulations (DNS) of both hydrodynamic (HD) and magnetohydrodynamic (MHD) decaying turbulence to classify different types by their decay behavior. The decay is characterized by the temporal change of the kinetic energy spectrum $E_K(k,t)$, and, in MHD, also by the magnetic energy spectrum $E_M(k,t)$. Here, $k$ is the wave number and $t$ is time. In addition to the decay laws of the energies $\mathcal{E}_i(t) = \int E_i(k,t)dk$, with $i = K$ or $M$ for kinetic and magnetic energies, there are the kinetic and magnetic integral scales

$$\xi_i(t) = \int_0^\infty k^{-1}E_i(k,t)dk \Big/ \int_0^\infty E_i(k,t)dk. \quad (1)$$

We quantify the decay by the instantaneous scaling exponents $p(t) \equiv d\ln\mathcal{E}/d\ln t$ and $q(t) \equiv d\ln\xi/d\ln t$. Thus, we study the decay behaviors by plotting $p(t)$ vs $q(t)$ in a parametric representation. The $pq$ diagram turns out to be a powerful diagnostic tool.

Earlier work [8,14,15] has suggested that the decay behavior, and thus the positions of solutions in the $pq$ diagram, depend on the exponent $\alpha$ for initial conditions of the form $E \sim k^\alpha e^{-k/k_0}$, where $k_0$ is a cutoff wave number. Motivated by earlier findings [2,11] of an inverse cascade in decaying MHD turbulence, Olesen considered the time-dependent energy spectra $E(k,t)$ to be of the form [15]

$$E(k,t) \propto k^\alpha \psi(k\xi(t)), \quad (2)$$

where $\xi(t) \propto t^q$ with $q$ being an as yet undetermined scaling exponent, and $\psi$ is a function that depends on the dissipative and turbulent processes that lead to a departure from a power law at large $k$. Moreover, the slope $\psi' \equiv d\psi/d\kappa$ with $\kappa = k\xi$ must vanish for $\kappa \to 0$. This turns out to be a critical restriction.

Olesen then makes use of the fact that the HD and MHD equations are invariant under rescaling, $x \to \tilde{x}\ell$ and $t \to \tilde{t}\ell^{1/q}$, which implies corresponding rescalings for velocity $u \to \tilde{t}\ell^{1-1/q}$ and viscosity $\nu \to \tilde{\nu}\ell^{2-1/q}$. Furthermore, using the fact that the dimensions of $E(k,t)$ are given by $[E] = [x]^3[t]^{-2}$, and requiring $\psi$ to be invariant under rescaling $E \to \tilde{E}\ell^{3-2/q} \propto \tilde{k}^\alpha \ell^{-\alpha}\psi$, he

 

finds from Eq. (2) that $\alpha = -3 + 2/q$. He argues that for a given subinertial range spectral exponent $\alpha$, the exponent $q$ is given by [12,15–17]

$$q = 2/(3+\alpha) \tag{3}$$

for both HD and MHD and independent of the presence or absence of helicity. A remarkable prediction of Olesen's original work concerns the existence of inverse transfer even in the absence of magnetic helicity, provided $\alpha > -3$. In subsequent work he stresses that for constant $\nu$ (and $\eta$), only the case $\alpha = 1$ can be realized. For nonhelical MHD, this is indeed compatible with simulations [18–20], but not for HD [21] or for helical MHD [3,22].

In this Letter, we argue that the scaling exponent $q$ is not primarily determined by the initial value of $\alpha$, as suggested by Eq. (3), but by the physical processes involved. Moreover, we relax the restriction $\psi'(0) = 0$ and write instead

$$E(k\xi(t), t) = \xi^{-\beta}\phi(k\xi), \tag{4}$$

where $\xi = \xi(t)$ is computed from Eq. (1), and $\beta$ needs to be determined empirically or theoretically. Clearly, the initial power law slope at small $k$ is no longer an adjustable input parameter, but is fixed by the form of $\phi = \phi(\kappa)$. Specifically, the "intrinsic" slope is $\alpha_* \equiv d\ln\phi/d\ln\kappa$. Evidently, $\psi$ can be computed from $\phi$ as $\psi(\kappa) = \xi^{\alpha-\beta}\phi(\kappa)/\kappa^{\alpha}$, but, in general, $d\ln\psi/d\ln\kappa = \alpha_* - \alpha \neq 0$ for $\kappa \to 0$.

In the following, we study examples of different decay behaviors in the diagnostic $pq$ diagram using data from DNS. As in earlier work [22], we solve the nonideal HD and MHD equations for an isothermal equation of state; i.e., the pressure $P$ and density $\rho$ are proportional to each other, $P = \rho c_s^2$, where $c_s = \text{const}$ is the sound speed. The kinematic viscosity $\nu$ is characterized by the Reynolds number, $\mathrm{Re} = u_{\rm rms}\xi/\nu$, with $u_{\rm rms} = (2\mathcal{E})^{1/2}$ and the magnetic diffusivity $\eta$ is characterized by the magnetic Prandtl number $\mathrm{Pr}_M = \nu/\eta$. The governing equations are solved using the Pencil Code [23,24]. The resolution is either $1152^3$ or $2304^3$ mesh points. The Mach number $u_{\rm rms}/c_s$ is always below unity, so compressibility effects are weak.

We first consider cases that have $\alpha = 4$ for the initial spectral slopes of $E_K$ or $E_M$. We consider (i) HD decay, (ii) nonhelical MHD decay, and (iii) helical MHD decay. In cases (ii) and (iii), the magnetic energy also drives kinetic energy through the Lorentz force. The particular simulation of case (ii) was already presented in Ref. [18], where inverse transfer to smaller wave numbers was found in the absence of magnetic helicity using high-resolution DNS. Case (iii) leads to standard inverse transfer [2,3,9,10]. The resulting spectra are plotted in Figs. 1(a)–1(c), where we show energy spectra for cases (i)–(iii) at different times. The values of the Re at half time are roughly 100, 230, and 300, respectively.

In Figs. 1(d)–1(f) we compare with suitably compensated spectra. We compensate for the shift in $k$ by plotting $E(k,t)$ against $k\xi(t)$. The peak in each spectrum, which is approximately at $k = \xi^{-1}$, has then always the same position on the abscissa. Furthermore, to compensate for the decay in energy, we multiply $E$ by $\xi^{\beta}$ with some exponent $\beta$ such that the compensated spectra collapse onto a single function $\phi(k\xi(t)) \approx \xi^{\beta}E(k\xi(t), t)$. In terms of the energy $\mathcal{E}(t) \equiv \int E(k,t)dk$, the function $\Phi = \xi^{\beta+1}\mathcal{E}_K$ is asymptotically constant, $\Phi(t) \to \Phi_\infty$, and has the same dimension as $\phi$, so we plot the nondimensional ratio $\phi/\Phi_\infty$. The function $\psi(\kappa)$ is shown as an inset and normalized by $\Psi_* \equiv \xi^{\alpha-\beta}\Phi$ at the last time.

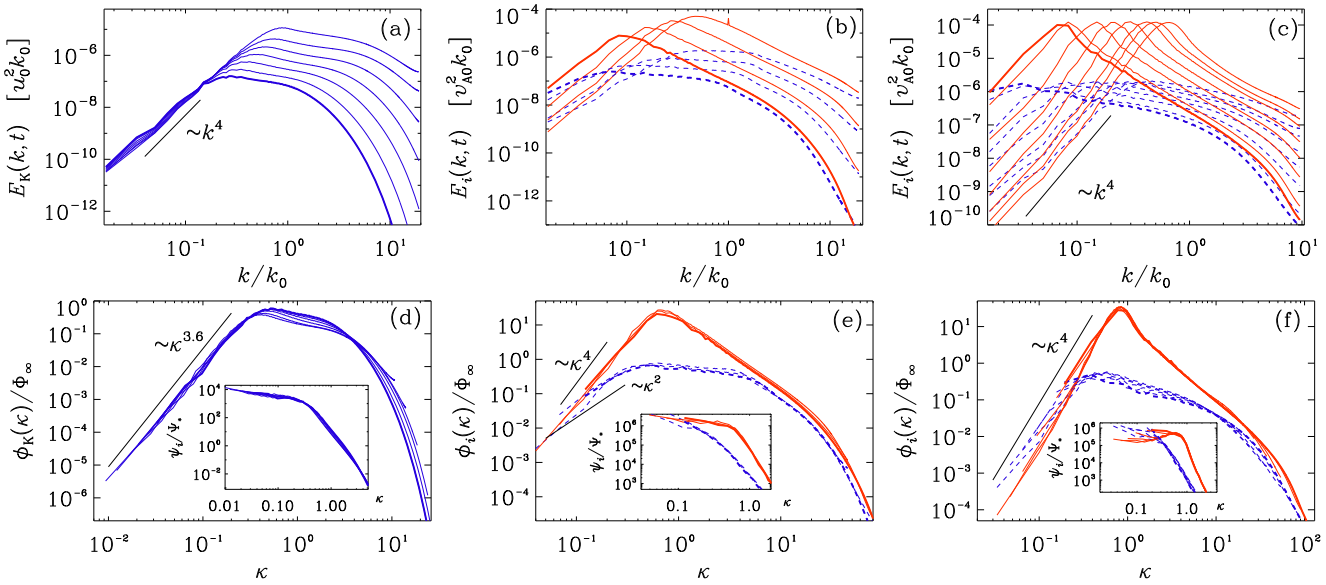


FIG. 1. $E_K(k,t)$ for different $t$ in HD DNS (a), compared with $E_M$ (solid red) and $E_K$ (dashed blue) in MHD without helicity (b), and with helicity (c). Panels (d)–(f) show collapsed spectra using $\beta = 3$ (d), $\beta = 1$ (e), and $\beta = 0$ (f).

Let us now consider solutions (i)–(iii) in the $pq$ diagram, see Figs. 2(a)–2(c). These are compatible with independently computed $\beta q$ diagrams [24]. To study the relation between the exponents $\beta$ and $q$, we make use of Olesen's scaling arguments and the fact that $\phi$ is invariant under rescaling, to show from Eq. (4) that $\beta + 3 - 2/q = 0$, i.e.,

$$\beta = 2/q - 3, \tag{5}$$

or $q = 2/(3+\beta)$. This is formally equivalent to Olesen's relation (3), but with $\alpha$ being replaced by $\beta$. Moreover, unlike the exponent $\alpha$ in Eq. (2), the exponent $\beta$ in Eq. (4) bears no relation with the initial spectral slope, except for certain cases discussed below. The temporal decay of kinetic and magnetic energies follows power laws $\mathcal{E}_i(t) \sim t^{-p_i}$ for $i = K$ or $M$. The exponents are obtained by integrating over $k$, $\mathcal{E}(t) = \xi^{-(\beta+1)} \int \phi d(k\xi) \propto t^{-p}$, and since $\xi \propto t^q$, this yields

$$p = (1+\beta)q. \tag{6}$$

Thus, in a $pq$ diagram, a certain value of $\beta$ corresponds to a line $p(t) \propto q(t)$ with the slope $\beta + 1$. Furthermore, inserting Eq. (5) yields the line $p = 2(1-q)$. We call this the self-similarity line.

The exponents $\beta$, $p$, and $q$ are roughly consistent with those expected based on the dimensions of potentially conserved quantities such as the Loitsiansky integral [27], $\mathcal{L} = \int \boldsymbol{r}^2 \langle \boldsymbol{u}(\boldsymbol{x}) \cdot \boldsymbol{u}(\boldsymbol{x}+\boldsymbol{r}) \rangle d\boldsymbol{r} \propto \ell^5 u_\ell^2$, with typical velocity $u_\ell$ on scale $\ell$, the magnetic helicity $\langle \boldsymbol{A} \cdot \boldsymbol{B} \rangle$, where $\boldsymbol{B} = \boldsymbol{\nabla} \times \boldsymbol{A}$ is the magnetic field in terms of the vector potential $\boldsymbol{A}$, and the mean squared vector potential $\langle \boldsymbol{A}^2 \rangle$, which is conserved in two-dimensions (2D); see Table I.

In the HD case (i), the solution approaches the $\beta = 3$ line and then settles on the self-similarity line at $q \approx 1/3$, see Fig. 2(a). This decay behavior departs from what would be expected if the Loitsiansky integral were conserved, i.e., $q = 2/7$ and $\beta = 4$. A slower decay law with $p = 6/5$, corresponding to $q = 2/5$ and $\beta = 2$, has been favored by Saffman [28], while experiments and simulations suggest $p = 5/4$ [21,29].

In case (ii), the solution evolves along $\beta = 1$ toward $q = 1/2$, see Figs. 2(b) and 2(e). This is compatible with the conservation of $\langle \boldsymbol{A}_{2\mathrm{D}}^2 \rangle$, where $\boldsymbol{A}_{2\mathrm{D}}$ is the component of $\boldsymbol{A}$ that describes the 2D magnetic field in the plane perpendicular to the local intermediate eigenvector of the rate-of-strain matrix $\mathbf{S}$, see the Supplemental Material [18] for details and also Ref. [30]. The motivation for applying 2D arguments to 3D comes from the fact that for sufficiently strong magnetic fields the dynamics tends to become locally 2D in the plane perpendicular to the local field. This allows one to compute $\boldsymbol{A}$ in a gauge that projects out contributions perpendicular to the intermediate eigenvector of $\mathbf{S}$.

TABLE I. Scaling exponents and relation to physical invariants and their dimensions.

| $\beta$ | $p$ | $q$ | Invariant | Dimension |
|---|---|---|---|---|
| 4 | $10/7 \approx 1.43$ | $2/7 \approx 0.286$ | $\mathcal{L}$ | $[x]^7[t]^{-2}$ |
| 3 | $8/6 \approx 1.33$ | $2/6 \approx 0.333$ | | |
| 2 | $6/5 = 1.20$ | $2/5 = 0.400$ | | |
| 1 | $4/4 = 1.00$ | $2/4 = 0.500$ | $\langle \boldsymbol{A}_{2\mathrm{D}}^2 \rangle$ | $[x]^4[t]^{-2}$ |
| 0 | $2/3 \approx 0.67$ | $2/3 \approx 0.667$ | $\langle \boldsymbol{A} \cdot \boldsymbol{B} \rangle$ | $[x]^3[t]^{-2}$ |
| $-1$ | $0/2 = 0.00$ | $2/1 = 1.000$ | | |

In case (iii) the solution evolves along $\beta = 0$. toward $q = 2/3$, see Figs. 2(c) and 2(f). This means that the spectrum shifts just in $k$, while the amplitude of $E_M$ does not change, as can be seen from Fig. 2(c). This is consistent with the invariance of $\langle \boldsymbol{A} \cdot \boldsymbol{B} \rangle$, see Ref. [3].

Next, we investigate cases with $\alpha < 4$. In the helical case with $\alpha = 2$ we see that the subinertial range spectrum quickly steepens and approaches $\alpha_* = 4 \neq \alpha$, see Figs. 3(a)–3(c). For $\alpha = -1$, which is a scale-invariant spectrum, the spectral energy remains nearly unchanged at small $k$, but the magnetic energy still decays due to decay at all higher $k$, see Figs. 3(d)–3(f). The values of $p_M$ and $q_M$ are rather small ($\approx 0.2$), but the spectra can still be collapsed onto each other with $\beta = 0$, see Fig. 3(e).

The examples discussed above demonstrate that in general $\beta \neq \alpha \neq \alpha_*$; i.e., the self-similarity parameter $\beta$ is not determined by the initial power spectrum but rather by the different physical processes involved. In helical MHD, we always find $\alpha_* = 4$ together with $\beta = 0$. For nonhelical MHD with $\alpha = 4$ and $E_K \propto k^2$, we find $\beta = 1$,

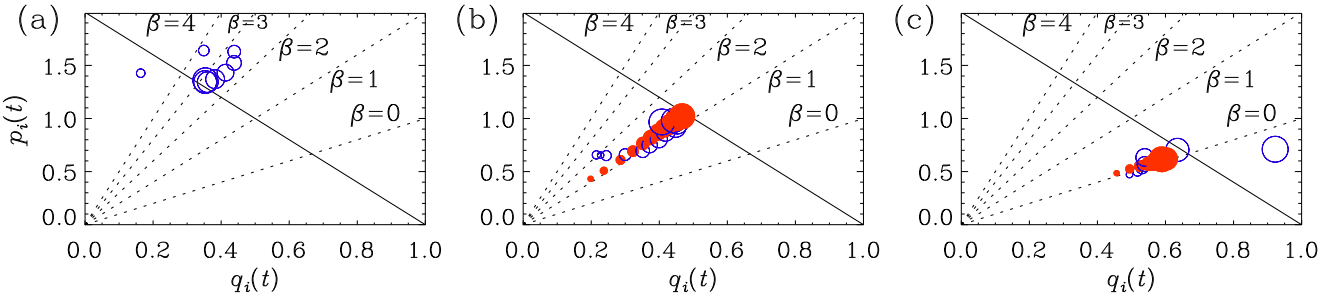


FIG. 2. $pq$ diagrams for cases (i)–(iii). Open (closed) symbols correspond to $i = K$ ($M$) and their sizes increase with time.

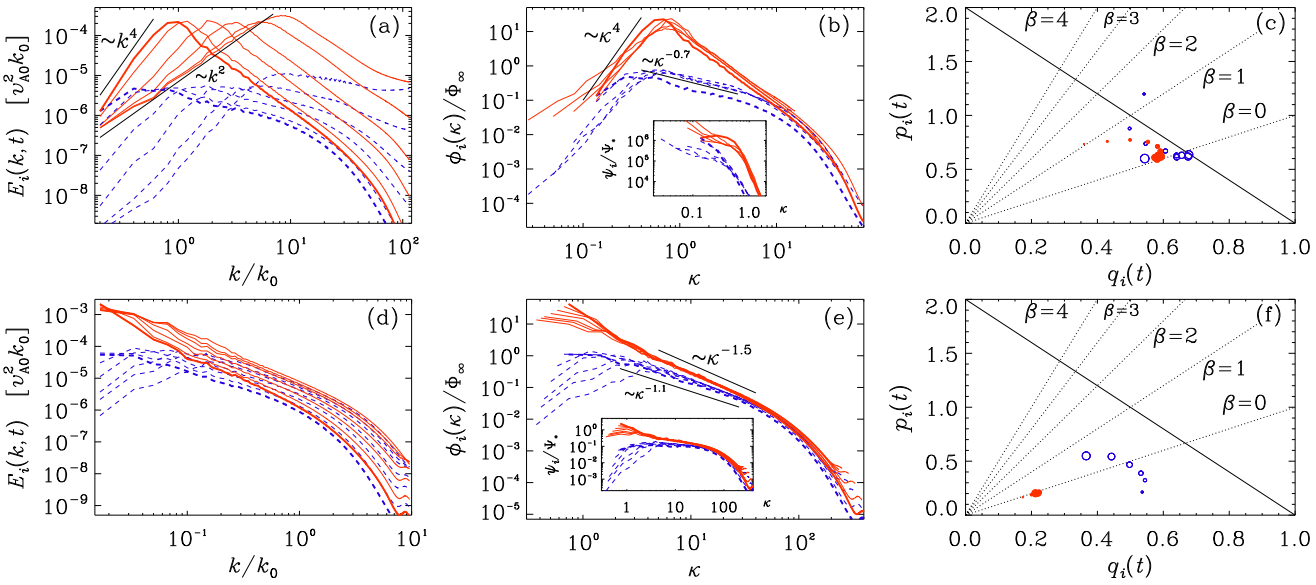


FIG. 3. $E_M$ (solid) and $E_K$ (dashed) in MHD with fractional helicity and $\alpha = 2$ (a), as well as full helicity and $\alpha = -1$ (d), together with compensated spectra (b),(e) and the $pq$ diagrams (c),(f).

while in HD with $\alpha = 4$, we find $\beta = 3$. In agreement with earlier work [31], the following exceptions can be identified: in HD with $1 \le \alpha \le 3$ and in nonhelical MHD with $1 \le \alpha \le$ we find $\beta = \alpha$ [24]. The only case where $\alpha = \beta = 4$ has been found is when the magnetic Prandtl number $\mathrm{Pr}_M \equiv \nu/\eta$ is small, see Figs. 4(a)–4(c) for $\mathrm{Pr}_M = 0.01$. Here, the conservation of $\mathcal{L}$ may actually apply [27]. For $\mathrm{Pr}_M \equiv \nu/\eta \gg 1$, on the other hand, we find $\beta = 2$ scaling, even though $\alpha = 4$, see Figs. 4(d)–4(f).

In conclusion, the present work has revealed robust properties of the scaling exponent $\beta$ governing the time dependence of the energy spectrum $E(k,t)$ through $\xi^\beta \phi(k\xi)$ with a time-independent scaling function $\phi$ and a time-dependent integral scale $\xi(t)$. The helical case is particularly robust in that any point in the $pq$ plane evolves along the $\beta = 0$ line $(p = q)$ toward the point $p = q = 2/3$. Furthermore, if the initial spectrum has $\alpha = 2$, it first steepens to $\alpha = 4$ and then follows the same decay as with an initial $\alpha = 4$. Moreover, for a scale-invariant spectrum with $\alpha = -1$, we again find $\beta = 0$, i.e., the same as for $\alpha = 2$ and 4, but now with $p_M \approx q_M \approx 0.2$, see Fig. 3(f). In the fractionally helical case, points in the $pq$ plane evolve

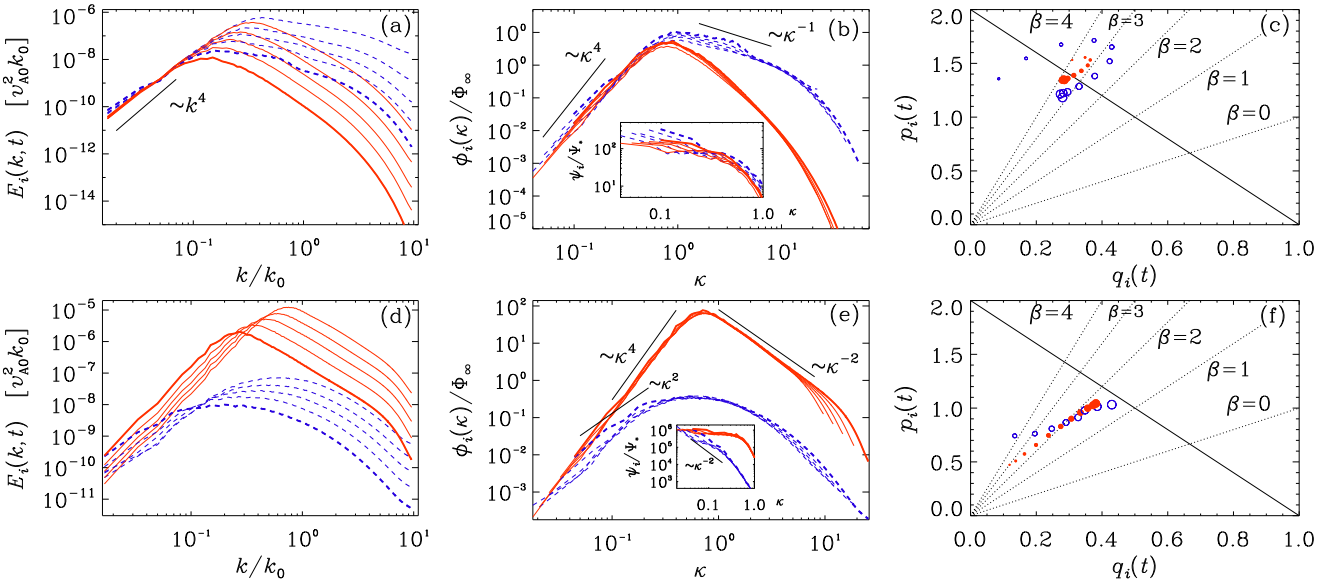


FIG. 4. Similar to Fig. 3, but for nonhelical MHD with $\mathrm{Pr}_M = 0.01$ (a) and $\mathrm{Pr}_M = 100$ (d), together with compensated spectra (b),(e) and the $pq$ diagrams (c),(f).

toward the $\beta = 0$ line and, for $\alpha \geq 2$, later toward $p_M = q_M = 2/3$.

Our results have consequences for two types of cosmological initial magnetic fields: causal ones with $E_M \propto k^4$ will always be accompanied by a shallower kinetic energy spectrum $E_K \propto k^2$, thus favoring inverse transfer [18,32], while a scale-invariant inflation-generated helical field exhibits self-similarity with $\beta = 0$ in the same way as for other initial slopes, but now with $p = q \approx 0.2$ instead of $2/3$. For decaying wind tunnel turbulence, Loitsiansky scaling is ruled out in favor of Saffman scaling, provided $\alpha = 2$. No inverse transfer is possible in HD, even if $\alpha = 4$, contrary to earlier claims [15]. The experimental realization of initial conditions with $\alpha \neq 2$ could be challenging for wind tunnels, but may well be possible in plasma experiments [33].

We thank Andrey Beresnyak, Leonardo Campanelli, Ruth Durrer, Alexander Tevzadze, and Tanmay Vachaspati for useful discussions. Support through the NSF Astrophysics and Astronomy Grant Program (Grants No. 1615940 and No. 1615100), the Research Council of Norway (FRINATEK Grant No. 231444), the Swiss NSF SCOPES (Grant No. IZ7370-152581), and the Georgian Shota Rustaveli NSF (Grant No. FR/264/6-350/14) are gratefully acknowledged. We acknowledge the allocation of computing resources provided by the Swedish National Allocations Committee at the Center for Parallel Computers at the Royal Institute of Technology in Stockholm. This work utilized the Janus supercomputer, which is supported by the National Science Foundation (Grant No. CNS-0821794), the University of Colorado Boulder, the University of Colorado Denver, and the National Center for Atmospheric Research. The Janus supercomputer is operated by the University of Colorado Boulder.

*brandenb@nordita.org
†tinatin@andrew.cmu.edu

[1] G. K. Batchelor and I. Proudman, Phil. Trans. R. Soc. A **248**, 369 (1956).
[2] A. Pouquet, U. Frisch, and J. Léorat, J. Fluid Mech. **77**, 321 (1976).
[3] D. Biskamp and W.-C. Müller, Phys. Rev. Lett. **83**, 2195 (1999).
[4] S. R. Stalp, L. Skrbek, and R. J. Donnelly, Phys. Rev. Lett. **82**, 4831 (1999).
[5] I. P. Castro, J. Fluid Mech. **93**, 631 (1979).
[6] D. K. Lilly, J. Atmos. Sci. **40**, 749 (1983).
[7] M.-M. Mac Low, R. S. Klessen, and A. Burkert, Phys. Rev. Lett. **80**, 2754 (1998).
[8] K. Subramanian, A. Shukurov, and N. E. L. Haugen, Mon. Not. R. Astron. Soc. **366**, 1437 (2006).
[9] M. Christensson, M. Hindmarsh, and A. Brandenburg, Phys. Rev. E **64**, 056405 (2001).
[10] R. Banerjee and K. Jedamzik, Phys. Rev. D **70**, 123003 (2004).
[11] A. Brandenburg, K. Enqvist, and P. Olesen, Phys. Rev. D **54**, 1291 (1996).
[12] L. Campanelli, Eur. Phys. J. C **76**, 504 (2016).
[13] J. M. Wagstaf and R. Banerjee, J. Cosmol. Astropart. Phys. 01 (2016) 002.
[14] W. K. George, Phys. Fluids **4**, 1492 (1992).
[15] P. Olesen, Phys. Lett. B **398**, 321 (1997).
[16] C. Kalelkar and R. Pandit, Phys. Rev. E **69**, 046304 (2004).
[17] L. Campanelli, Phys. Rev. D **70**, 083009 (2004).
[18] A. Brandenburg, T. Kahniashvili, and A. G. Tevzadze, Phys. Rev. Lett. **114**, 075001 (2015).
[19] J. Zrake, Astrophys. J. **794**, L26 (2014).
[20] P. Olesen, arXiv:1509.08962.
[21] H. S. Kang, S. Chester, and C. Meneveau, J. Fluid Mech. **480**, 129 (2003).
[22] A. G. Tevzadze, L. Kisslinger, A. Brandenburg, and T. Kahniashvili, Astrophys. J. **759**, 54 (2012).
[23] https://github.com/pencil-code.
[24] See Supplemental Material at http://link.aps.org/supplemental/10.1103/PhysRevLett.118.055102, which includes Refs. [25,26], for tests regarding the accuracy of the scheme and the assumption of isothermality and other properties of decaying MHD turbulence.
[25] A. Brandenburg and W. Dobler, Comput. Phys. Commun. **147**, 471 (2002).
[26] A. Brandenburg, in *The Fluid Mechanics of Astrophysics and Geophysics*, edited by A. Ferriz-Mas and M. Núñez, Advances in nonlinear dynamos (Taylor & Francis, London and New York, 2003), Vol. 9, pp. 269.
[27] P. A. Davidson, J. Fluid Mech. **663**, 268 (2010).
[28] P. G. Saffman, Phys. Fluids **10**, 1349 (1967).
[29] N. E. L. Haugen and A. Brandenburg, Phys. Rev. E **70**, 026405 (2004).
[30] P. Olesen, arXiv:1511.05007.
[31] T. A. Yousef, N. E. L. Haugen, and A. Brandenburg, Phys. Rev. E **69**, 056303 (2004).
[32] T. Kahniashvili, A. G. Tevzadze, A. Brandenburg, and A. Neronov, Phys. Rev. D **87**, 083007 (2013).
[33] C. B. Forest, K. Flanagan, M. Brookhart *et al.*, J. Plasma Phys. **81**, 345810501 (2015).